Michelle L. Burroughs
Department of Mechanical Engineering,
University of Utah,
Salt Lake City, UT 84112
e-mail: burroughs87@gmail.com

K. Beauwen Freckleton
Department of Mechanical Engineering,
University of Utah,
Salt Lake City, UT 84112
e-mail: bfreckleton@gmail.com

Jake J. Abbott
Mem. ASME
Department of Mechanical Engineering,
University of Utah,
Salt Lake City, UT 84112
e-mail: jake.abbott@utah.edu

Mark A. Minor[1]
Mem. ASME
Department of Mechanical Engineering,
University of Utah,
50 S Central Campus Dr, RM 2110,
Salt Lake City, UT 84112
e-mail: mark.minor@utah.edu

A Sarrus-Based Passive Mechanism for Rotorcraft Perching

This work examines a passive perching mechanism that enables a rotorcraft to grip branchlike perches and resist external wind disturbance using only the weight of the rotorcraft to maintain the grip. We provide an analysis of the mechanism's kinematics, present the static force equations that describe how the weight of the rotorcraft is converted into grip force onto a cylindrical perch, and describe how grip forces relate to the ability to reject horizontal disturbance forces. The mechanism is optimized for a single perch size and then for a range of perch sizes. We conclude by constructing a prototype mechanism and demonstrate its use with a remote-controlled (RC) helicopter.
[DOI: 10.1115/1.4030672]

1 Introduction

Flying robots, including rotorcraft and fixed-wing aircraft, have an increasing prevalence in a variety of applications because of their ability to gather useful information without the need for human presence. However, flying robots consume a great deal of power, yet have limited onboard energy resources. This makes hovering an inefficient method for data gathering. Perching on a structure (e.g., a tree branch and the roof of a building) enables a rotorcraft to gather information without consuming power, and even potentially recharge the energy source.

Our work aims to provide a passive perching mechanism so that a rotorcraft, such as a helicopter or quadrotor, is able to grip branchlike perches and resist external wind disturbances, using only the weight of the rotorcraft to maintain the grip. In our previous designs, we explored mechanisms inspired by the method used by songbirds to sleep while perching [1,2]. Songbirds have a tendon on the rear side of the ankle that allows them to automatically grip as the bird relaxes, with the weight of the bird causing the legs to bend, putting tension on the tendon, and causing the toes to grip. When the bird wants to take off, muscles are used to straighten the legs, releasing the grip.

In this paper, we propose a new mechanism that is neither avian-inspired nor tendon-based, but is designed to accomplish the same passive perching as our previous designs (Fig. 1). The new mechanism incorporates a Sarrus linkage to convert the weight of the rotorcraft into grip force. This one-degree-of-freedom mechanical linkage enforces linear translational motion between two parallel plates (Fig. 2) [3].

We use the linkage to convert the translational motion of the descent of the rotorcraft during a perching maneuver into angular motion of the connecting links with rigidly attached toes, resulting in a grip. Similarly, the translational ascent of the rotorcraft naturally releases the grip. The Sarrus linkage exhibits a high mechanical advantage in its collapsed state due to its proximity to a toggle point such that the downward force exerted by the rotorcraft's weight is amplified in the toes' grip.

In this paper, we begin with an analysis of the kinematics of our mechanism. We then present the static force equations that describe how the weight of the rotorcraft is converted into grip force onto a perch, and we describe how grip forces relate to the mechanism's ability to reject horizontal disturbances such as wind gusts. The mechanism is then optimized for use on a single given perch size. The optimization is then expanded to consider a range of perch sizes. We conclude by constructing a prototype mechanism, and we demonstrate its use with an RC helicopter.

Fig. 1 Our mechanism, shown here attached to the skids on the bottom of an RC helicopter, uses a bilateral configuration of Sarrus-based linkages to passively grip cylindrical perches

[1]Corresponding author.

Manuscript received November 3, 2014; final manuscript received May 14, 2015; published online August 18, 2015. Assoc. Editor: Satyandra K. Gupta.

2 Related Work

Many prior works have considered perching for either fixed-wing aircraft or rotorcraft, approached through various combinations of mechanism design, sensing, and control algorithms. Perching has been explored for a variety of surface orientations ranging from horizontal to vertical, and for a variety of surface geometries ranging from flat surfaces to cylindrical structures such as branches and power lines.

Some research on perching of fixed-wing aircraft has been largely based on sensing and control of the aircraft itself during a perching maneuver. Larson [4] developed an ultrasonic-distance-sensor-based embedded control system capable of executing vertical perching flight maneuvers in fixed-wing aircraft. Moore and Tedrake [5,6] developed a technique for perching at an incline on power lines using landing gear and magnetic localization. Hurst et al. [7], Hurst and Garcia [8], Gomez and Garcia [9], and Robertson and Reich [10] developed control schemes for morphing aircraft, which use bird-inspired wings and tails to perch on flat, horizontal surfaces.

In other research, perching of fixed-wing aircraft has been approached through the design of passive and active perching mechanisms. Several groups have used passive perching mechanisms attached to fixed-wing aircraft such as microspines, hooks, and adhesives. Desbiens et al. [11,12] and Glassman et al. [13] developed fixed-wing aircraft with microspines mounted on legs attached to the bottom of the wings to adhere to vertical surfaces. Anderson et al. [14] utilized a sticky pad dispenser attached to the nose of the fuselage to impact and adhere to vertical surfaces and then hang from a tether nose down. Cory and Tedrake [15] developed a fixed-wing robot with a latching hook that is used to perch on a horizontal string. Other groups have developed active mechanisms. Nagendran et al. [16] developed bio-inspired legs to grab and perch on flat, horizontal surfaces. Although not capable of grabbing a perch, Bachmann et al. [17] developed a leg-wheel crawling fixed-wing robot intended to land on a large horizontal surface area.

Researchers have also equipped rotorcraft with actuated perching mechanisms. Mellinger et al. developed an actuated gripper with opposing microspines that penetrate flat horizontal objects for perching and landing [18]. Kovač et al. [19] developed a perching system that uses the impact of the vehicle colliding with a vertical surface to snap barbs into the surface for perching, where actuation disengages and resets the barbs for the next perch. In other work, researchers have developed actuated mechanisms to be used for grasping, but which could also be used for perching on horizontal objects. Melinger et al. demonstrated grasping and transport [20] with their active perching mechanism [18] and subsequently developed a passively triggered spring-loaded grasper for transporting objects where servos open and reset the mechanism [21]. Pounds et al. [22] and Ghadiok et al. [23] developed underactuated compliant handlike graspers that enable a rotorcraft to grasp and carry an object during flight. Thomas et al. [24] recently equipped a quadrotor with an actuated arm capable of grasping objects at high horizontal speed, using an approach inspired by raptors.

A few groups have considered passive rotorcraft perching in a similar spirit to the work reported in this paper. Danko et al. [25] and Goldin [26] developed rotorcrafts with onboard sensors for autonomous perching on flat, horizontal surfaces, but with no dedicated perching mechanism. Daler et al. [27] developed a mechanism comprising fiber-based adhesive that enables perching on flat, vertical surfaces. In works that have a similar motivation to ours, Culler et al. [28] developed a gripping mechanism for a quadrotor, which uses a compliant snapping claw mechanism that is triggered upon landing on a branchlike structure. Although the mechanism proposed here is also intended for cylindrical branchlike structures, it can actually grip a range of perch shapes and it is quite different from related work since it relies solely upon gravitational forces to close the gripper and exert sufficient forces to grasp the perch. The mechanism is very lightweight, but its passive nature does mean that sufficient upward winds or lift due to horizontal winds could release the grasp, which may not be as significant in the actuated mechanisms described above. While in the same passive spirit as our prior work [1,2], the Sarrus mechanism proposed here is different: it is more of a traditional linkage whereas our prior work used tendons wrapped around knees to create actuation. This mechanism also uses rigid toes to grasp the perch whereas Refs. [1] and [2] used rubber toes that provided

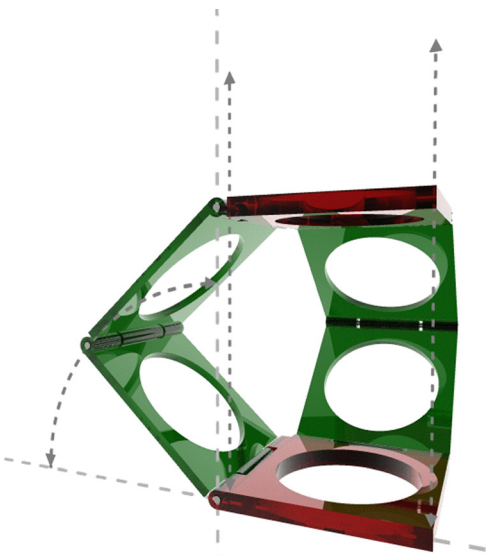

Fig. 2 A Sarrus linkage converts the pure translational motion between the top and bottom plates into angular motion of the plates in the connecting linkages. The two connecting linkages must be out-of-plane to keep the top and bottom plates parallel. Public domain image [3].

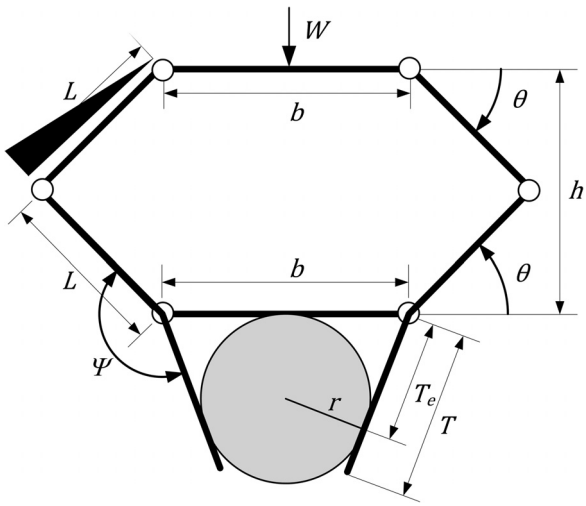

Fig. 3 Kinematic description of the Sarrus-based perching mechanism considered in this paper, with the rotorcraft's weight *W* causing the mechanism to grip on a cylindrical perch of a radius *r*. The mechanism is described by a set of constant geometric parameters: *b*, *L*, *T*, and Ψ. The mechanism is symmetric, and an out-of-plane linkage that is identical to the two side linkages (not shown) enforces that the top and bottom plates remain parallel as in Fig. 2. An additional set of parameters are used to describe the configuration of the mechanism on a given perch: θ, *h*, and T_e. Pin joints are indicated with small circles. Note that a bottom-side link and a toe form a single rigid link joined to the bottom plate with a pin joint.

restoring forces, but wasted force to actuate the toes. Since the mechanism in Ref. [1] and [2] is at a different scale and fundamentally different, it is difficult to say whether one is better than the other. The mechanism proposed here, however, seems to be easier to manufacture since it uses 3D printing, it is much lighter, and it is more compact. This paper contributes optimization processes for the mechanism and provides validating data.

3 Kinematic and Static Analysis

We first describe the concept of our proposed mechanism and its governing kinematic equations. Static equations describing how the weight of the rotorcraft is converted into grip force between the mechanism and the perch are as follows. Finally, resulting grip force is related to maximum applied horizontal disturbance force, such as that due to wind on the rotorcraft that can be successfully rejected.

3.1 Kinematic Analysis. Our Sarrus-based perching mechanism (Fig. 3) is described through a set of constant geometric parameters, which include base length, b, link length, L, rigid toe angle, Ψ, and toe length T. For configuration described in this paper, the mechanism is symmetric, with the top and bottom plates assumed to be of equal length, and the top and bottom side links assumed to be of equal length, these assumptions could be relaxed in future work. The top and bottom plates always remain parallel throughout the perching maneuver, which is enforced by an out-of-plane linkage that is identical to the two side linkages shown in Fig. 3, as in Fig. 2, but without the toe.

Additional parameters describe the configuration of the mechanism when collapsed on a perch. The effective toe length T_e describes the length of the toe between the bottom joint and the toe's contact point with the perch. The grip angle θ describes the angle between the bottom side link and the horizontal. $\theta = 0$ and $\theta = \pi/2$ rad both correspond to toggle positions in the mechanism that should be avoided. The height, h, defines the distance between the top and bottom plates. The grip angle is related to the height through the link length, L, using the law of cosines

$$h = 2L\sin(\theta) \Leftrightarrow \theta = \sin^{-1}\left(\frac{h}{2L}\right) \tag{1}$$

To find the location where the toe contacts the perch, we define a new angle β, the toe contact angle (Fig. 4). To solve for β, we analyze symmetric halves of the area between a toe and the bottom plate through an angle α (Fig. 4). Geometrically, the angle α is a function of the base length, b, and the perch radius, r

$$\alpha = \tan^{-1}\left(\frac{2r}{b}\right) \tag{2}$$

To solve for the toe contact angle, β, we relate the Cartesian coordinates of the toe contact point to the angle α, base length b, and perch radius r

$$x_\beta = \frac{b}{2}\cos(2\alpha) \tag{3}$$

$$y_\beta = \frac{b}{2}\cos(2\alpha) \tag{4}$$

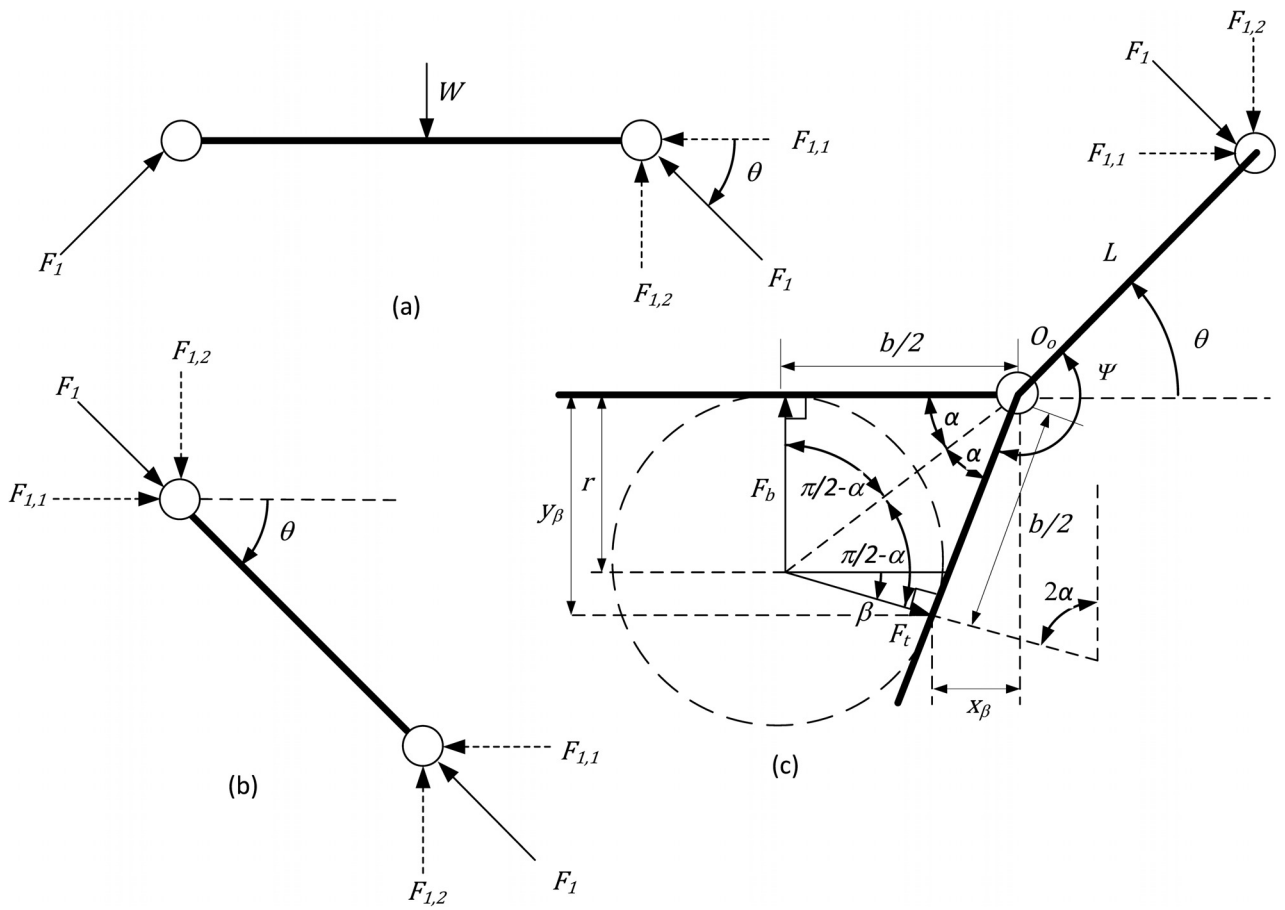

Fig. 4 Right side of symmetrical Sarrus-based perching mechanism, broken into three components: (*a*) the top plate, (*b*) the top side linkage, and (*c*) the bottom half of the mechanism, which includes the bottom side linkage and its rigidly attached toe, attached to the bottom plate at a pin joint. Small circles represent pin joints.

$$\beta = \tan^{-1}\left(\frac{x_\beta}{y_\beta}\right) \tag{5}$$

After substitution and simplification, β is based on known parameters

$$\beta = \frac{\pi}{2} - 2\tan^{-1}\left(\frac{2r}{b}\right) \tag{6}$$

The equation for the toe contact angle, β, is only a function of one dimensionless variable: the ratio of the perch diameter to the base length. The solution becomes degenerate when the perch diameter is equal to the base length; for this trivial case, $\beta = 0$. The grip angle θ is related to the toe contact angle β through the rigid toe angle Ψ as

$$\theta = \Psi - \beta - \frac{\pi}{2} \tag{7}$$

Because the toe's contact point and bottom plate's contact point are equidistant from joint O_o, the effective toe length is $T_e = b/2$ for any perch size. It is clear that the largest perch size that can be surrounded and gripped by the toes as shown in Fig. 3 is bounded by $r = b/2$, which is intuitive for straight toes.

3.2 Static Grip Analysis. Understanding the kinematic configuration of the perching mechanism, a static analysis now relates the weight of the rotorcraft to the grip force that the mechanism applies to the perch. The mechanism is deconstructed into two symmetrical halves, and the right side is analyzed to find the forces throughout the linkage (Fig. 4). The force acting between the top plate and the top side link is F_1, which is decomposed into Cartesian force components $F_{1,1}$ and $F_{1,2}$. Forces are positive when in compression. A static force and moment balance on the top side link (Fig. 4(*b*)) highlights that F_1 must be directed along the link since its pin joints cannot support a moment. Therefore, F_1 is applied to the top plate at the grip angle θ (Fig. 4(*a*)). Using a static force balance on the top plate, solve for F_1 and its Cartesian components as a function of the rotorcraft's weight W.

$$F_{1,2} = \frac{W}{2} = F_1 \sin(\theta s) \tag{8}$$

$$F_1 = \frac{W}{2\sin(\theta)} \tag{9}$$

$$F_{1,1} = \frac{F_{1,2}}{\tan(\theta)} = \frac{W}{2\tan(\theta)} \tag{10}$$

Moment analysis of the bottom side link (Fig. 4(*c*)), thus results in

$$F_t\left(\frac{b}{2}\right) - F_{1,1}(L\sin(\theta)) - F_{1,2}(L\cos(\theta)) = 0 \tag{11}$$

With internal linkage forces expressed in terms of the weight of the rotorcraft and the grip angle, use a moment balance about joint O_o to find the compressive force F_t that the toe applies to the perch. These results in an equation for the force that a toe applies to the perch, where the weight, W, enters linearly

$$F_t = W\left(\frac{2L}{b}\cos(\theta)\right) \tag{12}$$

and θ is a function of known parameters (Eq. (7)).

We have assumed that there is one toe on each side of the perch, but, in general, there could be several toes on a given side of the perch such that F_t would be distributed equally between the toes.

To find the compressive force F_b that the bottom plate applies to the perch, perform a static force balance on the bottom plate. The vertical force F_b must be shared equally between the two bottom plate pin joints due to symmetry. A static force balance in the vertical direction on the bottom side link provides

$$\frac{F_b}{2} - F_{1,2} - F_t\sin(\beta) = 0 \tag{13}$$

$$F_b = W\left(1 + 2\left(\frac{2L}{b}\right)\cos(\theta)\sin(\beta)\right) \tag{14}$$

with β and θ defined as functions of mechanism parameters in Eqs. (6) and (7), respectively. Just as $(2r/b)$ was found to be important for characterizing the toe contact angle β, the parameter $(2r/b)$ is important for characterizing the grip force of the mechanism, both from the toes and the bottom plate.

F_b should remain positive (i.e., in compression) to ensure that the bottom plate maintains in contact with the perch so that it contributes to the grip and so that our analysis remains valid. This requires

$$\cos(\theta) > -\frac{b}{4L\sin(\beta)} \tag{15}$$

This condition is always satisfied when β is constrained to be in the range $0 < \beta < \pi/2$ by design, assuming that β falls within the normal operating range of the Sarrus linkage: $0 < \theta < \pi/2$. Enforcing this assumption requires that we constrain Ψ for any given β to the range

$$\beta + \frac{\pi}{2} < \Psi < \beta + \pi \tag{16}$$

We will find in Sec. 4 that as our range of desired perch sizes (and thus, the range of expected β) increases, our range of acceptable Ψ values decreases.

3.3 Disturbance Rejection. Grip forces between the mechanism and the perch are now related to the ability of the mechanism to reject horizontal disturbance forces (e.g., wind) on the rotorcraft. Vertical disturbance forces are not included here since they directly increase or decrease the effective weight, W, applied to the mechanism, which is already considered above. Assume that a disturbance force F_D is applied horizontally at some distance a above the top plate (e.g., at the center of pressure of the rotorcraft), which creates a disturbance moment about the perch

$$M_D = F_D(a + h + r), \tag{17}$$

that must be counteracted by the grip (this equation assumes negligible thickness of the top and bottom plates). Assume coefficient of static friction μ at the perch-mechanism interface. The maximum static moment that can be rejected by the grip forces, which act at a moment arm r, is given by

$$M_{D,max} = \mu r(F_b + 2F_t) \tag{18}$$

which, after substitutions, becomes

$$M_{D,max} = \mu W r\left(1 + \left(\frac{4L}{b}\right)\cos(\theta)(1 + \sin(\beta))\right) \tag{19}$$

Our mechanism will be able to reject any disturbance moment that is less than this maximum: $M_D < M_{D.max}$. We can combine the above equations to solve for the upper bound on the horizontal disturbance force that can be rejected

$$F_{\mathrm{D,max}} = \frac{\mu W r\left(1 + \left(\frac{4L}{b}\right)\cos(\theta)(1+\sin(\beta))\right)}{a + 2L\sin(\theta) + r} \tag{20}$$

with β and θ defined as functions of mechanism parameters in Eqs. (6) and (7), respectively. Note that the rotorcraft's weight, W, and the coefficient of static friction, μ, are linear. Equipped with an equation that describes the maximum disturbance force that can be rejected as a function of the mechanism parameters, we now optimize the mechanism to improve robustness to disturbances.

4 Design and Optimization

In this section, we describe the process of defining the optimal perching mechanism, first for a single perch, and then for a specified range of perch sizes. Mechanism parameters including link lengths (e.g., L, b, and a) relative to perch radius, r, rigid toe angle, Ψ, and minimum angle of the mechanism, $\theta_{\min}$, are considered.

4.1 Optimization for a Single Perch Size. To optimize for a single perch size, we first define the range of parameters for which the mechanism/rotorcraft system will achieve a valid grasp (as depicted in Fig. 3). Then, we examine each parameter individually, and find an optimal solution that maximizes the disturbance force that can be rejected.

Before performing the optimization of our mechanism, we first recognize that the rotorcraft's weight and the coefficient of friction between the toes and the perch both enter into the maximum disturbance force linearly, and we can therefore optimize a nondimensional maximum disturbance force

$$\tilde{F}_{\mathrm{D}} = \frac{F_{\mathrm{D,max}}}{\mu W} \tag{21}$$

Note we drop the "max" subscript in the nondimensional variable for brevity. We can also normalize our various length parameters by the perch radius, which can be seen by dividing both the numerator and denominator of Eq. (20) by r

$$\tilde{L} = \tfrac{l}{r}, \quad \tilde{b} = \tfrac{b}{r}, \quad \tilde{a} = \tfrac{a}{r} \tag{22}$$

The result is a fully nondimensional equation for the maximum disturbance force that can be rejected

$$\tilde{F}_{\mathrm{D}} = \frac{4\tilde{L}\cos(\theta)(1+\sin(\beta)) + \tilde{b}}{\tilde{a}\tilde{b} + 2\tilde{L}\tilde{b}\sin(\theta) + \tilde{b}} \tag{23}$$

Our goal during optimization will be to maximize this quantity.

First, we consider the effect of the normalized link length $\tilde{L}$. In the limit as $\tilde{L}$ becomes very small, the perching mechanism has no role in rejecting a disturbance force, and the rotorcraft is essentially balancing atop the perch

$$\lim_{\tilde{L}\to 0} \tilde{F}_{\mathrm{D}} = \frac{1}{\tilde{a}+1} \tag{24}$$

In the limit as $\tilde{L}$ becomes very large, there is an upper bound to the force that can be rejected

$$\lim_{\tilde{L}\to 0} \tilde{F}_{\mathrm{D}} = \frac{2(1+\sin(\beta))}{\tilde{b}\tan(\theta)} \tag{25}$$

As we increase the link length, the disturbance force that can be rejected increases, but there is a diminishing return as we asymptotically approach the upper bound in Eq. (25). Since an increase in link length will have an accompanying increase in weight that must be lifted by the rotorcraft, we must be conscientious of this trade-off. In the general case, where link length is neither extremely short nor extremely long, the relationship between the various design parameters and the maximum disturbance force is nontrivial.

We see that (at least for very long link lengths) there is clear push to minimize the grip angle θ to increase disturbance rejection, which is not confounded by other factors. This corresponds to the mechanism collapsing down into its toggle position. Because of the high mechanical advantage near the toggle position, the weight of the rotorcraft could potentially deform the links or joints and violate the fundamental kinematics of the mechanism. Therefore, we introduce a new design parameter: the minimum grip angle $\theta_{\min}$. This parameter establishes how close we will allow the mechanism to get to its fully collapsed toggle position (i.e., horizontal). We will use the same angle to establish how close we will allow the mechanism to get to its fully open toggle position (i.e., vertical) when the mechanism hangs below the rotorcraft; in future work, these values could be set independently.

We must now update our relationship for the allowable rigid toe angle from Eq. (16) to account for the user-defined minimum grip angle. We will also incorporate our solution for β from Eq. (6), as well as our Ψ normalization of Eq. (23). The resulting limit on Ψ is

$$\pi - 2\tan^{-1}\left(\frac{2}{\tilde{b}}\right) + \theta_{\min} < \Psi < \frac{3\pi}{2} - 2\tan^{-1}\left(\frac{2}{\tilde{b}}\right) - \theta_{\min} \tag{26}$$

The size of the maximum range of acceptable rigid toe angles Ψ is thus always $(\pi/2 - 2\theta_{\min})$ for any given perch size, with the values for the base length $\tilde{b}$ and minimum grip angle $\theta_{\min}$defining the boundaries of this range. As an example, consider a base length $\tilde{b} = 2$(in which the base length is equal to the diameter of the perch) and a minimum grip angle $\theta_{\min} = 0$: the range of acceptable toe angles is from $\pi/2$ to π rad and the corresponding range for the toe contact angle β is from 0 to $\pi/2$ rad. As the size of the desired perch decreases relative to the base length, but with the minimum grip angle maintained at $\theta_{\min} = 0$, the lower bound on acceptable Ψ evolves toward π radians, with the size of the range remaining as $\pi/2$ rad.

To perform an optimization in which the design parameters can be varied simultaneously, we utilize the MATLAB optimization function FMINCON to implement our governing equations and use normalized force disturbance as our metric to be maximized. With our understanding that the optimization routine will always drive $\theta_{\min}$ to zero and will always drive $\tilde{L}$ forever upward, we remove those quantities from the optimization and simply set them at constant values of $\tilde{L} = \tilde{b}/2$ and $\theta_{\min} = \pi/18$ rad. In the optimization, we use many randomly chosen initial conditions, which are first checked for validity, and then allow the numerical convergence to occur. Convergence always occurs to the same optimal parameter set, regardless of the initial condition. We find that the optimal normalized base length is $\tilde{b} = 2$, and as per Sec. 3.1, the toe contact angle becomes $\beta = 0$, such that the optimal rigid toe angle is described by the function

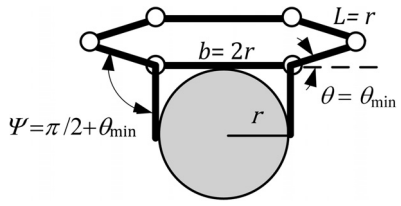

Fig. 5 Optimal design for a single perch radius, *r*. The link length *L* and grip angle $\theta_{\min}$ are set arbitrarily.

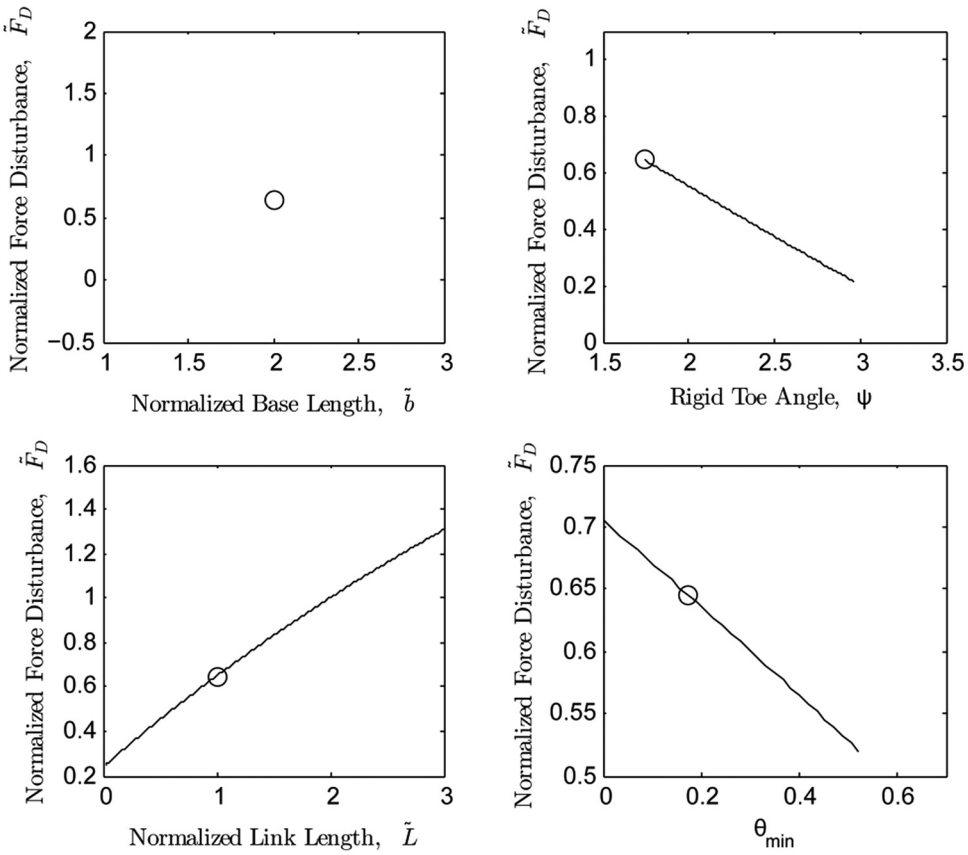

Fig. 6 Effect of varying individual parameters on the normalized force disturbance $\tilde{F}_D$, starting from the optimized design of Fig. 5. The parameters varied include: $\tilde{b}$, Ψ(rad), $\tilde{L}$, and θ_{min} (rad). The optimized design is indicated with a circle (the choices of $\tilde{L}$ and θ_{min} are still user-defined and arbitrary). Each parameter is varied individually while holding all other parameters at the initial values ($\tilde{b} = 2, \tilde{L} = 1, \theta_{min} = \pi/18$ rad, and $\tilde{a} = 3.255$).

$$\Psi_{optimal} = \frac{\pi}{2} + \theta_{min} \tag{27}$$

The optimal design is depicted in Fig. 5. In the optimal design, the mechanism's base length is equal to the diameter of the perch, resulting in the toes gripping the perch on the sides, and the rigid toe angle is such that the toes contact the perch at the instant when the mechanism has collapsed as close to the toggle position as is allowed by θ_{min}. Figure 6 shows the results of varying each design parameter one by one, starting from the optimized design, while holding the remaining parameters constant. As part of the "optimized" design, we arbitrarily select $\tilde{L} = \tilde{b}/2$ and $\tilde{a} = 3.255$ (this value is chosen because it is the actual value of our experimental case study used later). From the optimized design, we see that it is neither possible to increase nor decrease $\tilde{b}$ and still get a valid mechanism; decreasing $\tilde{b}$ would prohibit the toes from enclosing the perch, and increasing $\tilde{b}$ would result in the toes not making contact with the perch. It is possible to increase the rigid toe angle, but it would result in an inferior mechanism. As expected, we would still realize improved disturbance rejection by increasing $\tilde{L}$ or decreasing θ_{min}.

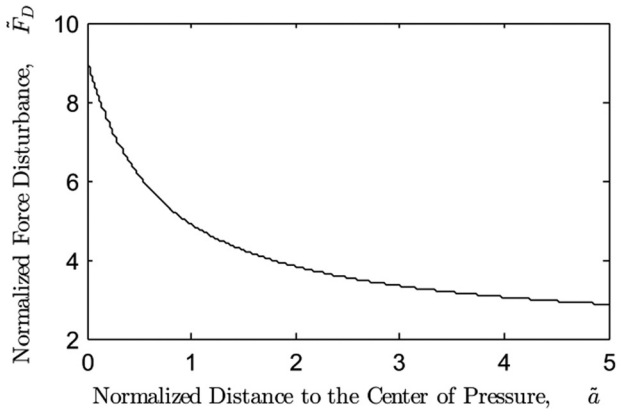

Fig. 7 Normalized force disturbance $\tilde{F}_D$ versus distance to the center of pressure $\tilde{a}$ (with $\tilde{b} = 2$, $\theta_{min} = \pi/18$ rad, and $\tilde{L} = 1$)

Figure 7 shows how the distance to the center of pressure $\tilde{a}$ affects the force disturbance that can be rejected. This parameter is a function of the aerodynamic properties of the rotorcraft, as well as the radius of the perch, and is thus not actually a mechanism design parameter that can be optimized. However, we should understand the role of this parameter on our mechanism's ability to reject disturbances. We observe that significant increases in disturbance rejection can be achieved if the distance between the center of pressure and the top of the perching mechanism can be minimized.

4.2 Optimizing for a Range of Perch Sizes. Rather than designing a mechanism that is optimized to perch on a single perch, it is probably more desirable to be able to perch on an entire inclusive range of perch sizes. To optimize for a range of perch sizes, we first define the range of parameters for which the mechanism/rotorcraft system will achieve a valid grasp (as depicted in Fig. 3) throughout the entire range. We then use our knowledge gained during the optimization for a single perch to inform our optimization for a range of perch sizes. We continue to

use the normalized force disturbance $\tilde{F}_D$ that can be rejected as our design metric that is to be maximized.

To consider a range of perch sizes, we will normalize the radius of a given perch in the range relative to the radius of the largest perch in the range, such that every perch in the range is described by a dimensionless scaling parameter $s \in (0, 1]$. Thus, the largest perch in the range is always represented by $s = 1$ and all smaller perches are represented by some $0 < s < 1$.

We learned two important facts in Sec. 4.1 about optimizing the mechanism for a given perch. First, we learned that the base b should be made as small as possible, which also makes the effective toe length as small as possible. For a range of perch sizes, the smallest base length that will result in valid perches throughout the entire range is achieved by choosing the base equal to the diameter of the largest perch in the range $\tilde{b} = 2$.

Second, we learned that it is always desirable to minimize the grip angle θ, both to increase the mechanical advantage of the mechanism and to reduce the moment arm of any force disturbances due to wind. Avoiding the mechanism's toggle positions throughout an entire range of perch sizes is achieved by choosing the grip angle to be equal to the minimum grip angle $\theta_{\min}$ for the smallest perch in the range. The result is that the grip angle on all other larger perches in the range will be larger than the minimum grip angle, due to the need of the mechanism to expand to accommodate larger perches. Recall that $\theta_{\min}$ is set by the designer to avoid the mechanism's toggle positions. A consequence of breaching toggle positions includes losing the free movement of mechanism needed for both ascent and descent. Thus, we must also ensure that the largest perch in a given range does not cause the mechanism to breach the fully open toggle position, which we will also choose to avoid by the same $\theta_{\min}$ (although a different value could be used, considering the different loading conditions on the mechanism in the two toggle positions). Avoiding these two toggle positions, taken together, restricts the range of perch sizes that can be gripped by a given mechanism. Since the grip angle for the largest perch in the range is always $\beta = 0$, the grip angle for the smallest perch, β_{small}, is equal to the total θ swept out from the largest to the smallest perch, which in turn is limited by avoiding the upper and lower toggle positions. Thus, the smallest perch that can be gripped for a given designer-specified $\theta_{\min}$ is calculated as

$$s_{\min} = \tan\left(\frac{\max \beta_{\text{small}}}{2}\right)\frac{\tilde{b}}{2} = \tan\left(\frac{\frac{\pi}{2} - 2\theta_{\min}}{2}\right)\frac{\tilde{b}}{2} \tag{28}$$

Figure 8 shows how setting a more conservative (i.e., larger) minimum grip angle restricts the range of perch sizes that can be gripped, this will be seen again in Fig. 11.

Figure 9 shows the nonlinear relationship between the maximum normalized force disturbance, $\tilde{F}_D$, that can be rejected through an inclusive range of perch sizes, for four different ranges. A range of perch sizes are denoted by $s = [s_{\text{small}}\ s_{\text{large}}]$. We observe that increasing the size of the range results in a decrease in the force disturbance that can be rejected on the largest perch in the range, with a nearly symmetric corresponding increase in the disturbance that can be rejected on the smallest perch in the range. We also observe that the median disturbance that can be rejected, which occurs at approximately the median perch size within a given range of perch sizes, is quite insensitive to the size of the range. Although the normalized force disturbance values reported in the figure are a function of three somewhat-arbitrary parameters $\tilde{L}$, $\theta_{\min}$, and $\tilde{a}$, the overall trends remain the same for different values.

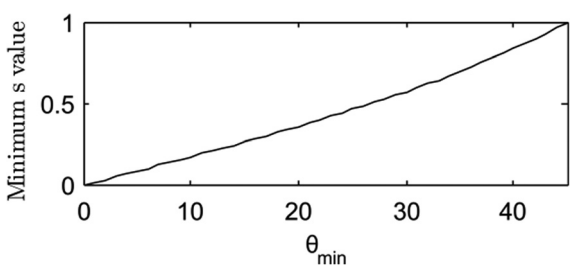

Fig. 8 Minimum relative perch size s versus minimum grip angle $\theta_{\min}$ (deg) with $\tilde{b} = 2$

In Fig. 10, we consider the effect of varying the normalized link length $\tilde{L}$ on the maximum normalized force disturbance $\tilde{F}_D$, using the same ranges of perch sizes shown in Fig. 9. Note the values reported at $\tilde{L} = 1$ are the same as those reported in Fig. 9. As expected, we observe that increasing the link length increases the force disturbance that can be rejected across designs. However, we also observe that the increases in disturbance rejection are greater at the small end of the perch-size range with increased sensitivity to link length as the range of perch sizes increases, and less pronounced at the large end of the perch-size range with decreased sensitivity to link length as the range of perch sizes increases. We observe that the difference in disturbance-rejection capability between the smallest and largest achievable perches within a given optimized range increases with increasing link length. This seems to confirm the significant effect in lowering the effective moment arm of the force disturbance about the perch by decreasing the smallest perch size, which allows the mechanism to settle deeper into the perch.

In Fig. 11, we consider the effect of varying the minimum grip angle $\theta_{\min}$ on the maximum normalized force disturbance $\tilde{F}_D$, using the same ranges of perch sizes shown in Fig. 9. Note the values reported at $\theta_{\min} = 10$ deg are the same as those reported in Fig. 9. We see that the smaller perch's force disturbance always exceeds that of the larger perch as expected. We also see that decreasing the $\theta_{\min}$ will always result in an increase in disturbance-rejection capability, as expected.

We summarize the optimal design process for a range of perch sizes as follows:

(1) Set the base length b equal to the diameter of the largest perch in the range (make it slightly larger for a small factor of safety).
(2) Set the toe length T to be equal to the radius of the largest perch in the range (make it slightly larger for a small factor of safety).
(3) Choose the minimum grip angle $\theta_{\min}$ to be as small as allowable to avoid toggle positions, ideally based on strength and tolerance analysis of the resulting mechanism.

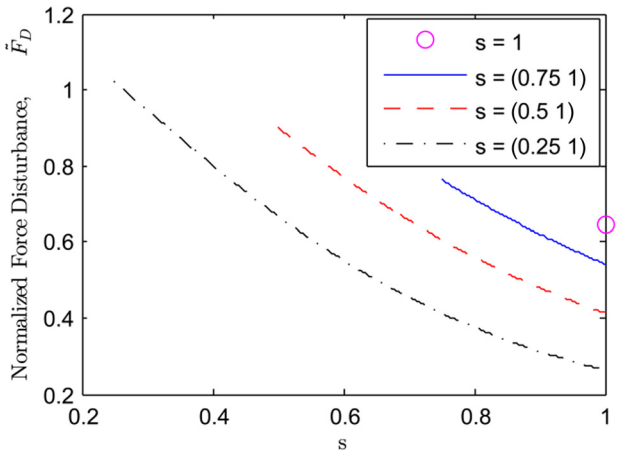

Fig. 9 Normalized force disturbance versus relative perch size for four different mechanisms that have each been optimized for a specified range of perch sizes (with $\tilde{L} = 1, \theta_{\min} = \pi/18$ rad, and $\tilde{a} = 3.255$ in all cases). The "range" $s = 1$ corresponds to the optimal design for a single perch size.

(4) Set the grip angle θ to be equal to $\theta_{\min}$ on the smallest perch in the range.
(5) Set the rigid toe angle Ψ based on the b value and the θ value for the smallest perch, using Eqs. (6) and (7).
(6) Choose the link length L to be as large as possible, given payload constraints.
(7) Mount the perching mechanism on the rotorcraft such that effective kinematic "top plate" of the mechanism is as high as possible in order to minimize its distance to the center of pressure of the rotorcraft.

5 Prototype and Experimental Verification

Using a Sky Crawler RC helicopter (Excalibur, Yonkers, NY), we utilized the procedures for finding the optimal perching mechanism for a range of perch sizes to create a prototype. First, we gathered wind-tunnel data to get a sense of how wind speed correlates with drag force to which the helicopter/mechanism system will be subjected. Drag is modeled as a quadratic function of wind speed: $F_D = C_D v^2$ with coefficient $C_D = 3.00 \times 10^{-3}$ N s/m based upon experimental tests [29]. Then, we experimentally estimate the vertical location of the center of pressure, $a = 62$ mm, using a plumb experiment in which we hang the system from two points where a is located at the intersection of the two plumb lines. Our complete mechanism mass is constrained given the experimentally determined 30 g payload limit of the Sky Crawler. Using the values found for this specific helicopter, we designed and constructed the optimal mechanism for a range of perch sizes.

We designed our mechanism for use on a range of perches in which the largest perch has a diameter of 42 mm ($r = 21$ mm), which corresponds to a dimensionless perch size of $s = 1$ by definition, and the smallest perch has a diameter of 21 mm ($r = 10.5$ mm), which corresponds to a dimensionless perch size $s = 0.5$. The perches we use here are made of polyvinyl chloride (PVC) pipe, which is available in a variety of diameters. This range of diameters is motivated by potential urban, industrial, and agricultural applications where this range of sizes might be typical (e.g., pipes, power lines, branches, man-made perches, etc.).

We chose our $\theta_{\min}$ iteratively through a series of prototypes and pilot tests. We settled on a $\theta_{\min} = 0.262$ rad (15 deg) because we found that if we allowed the mechanism to collapse beyond that value, the compliance in the links and joints would sometimes allow the mechanism to violate the fully collapsed toggle position. This same $\theta_{\min}$ was more than sufficient to prohibit the mechanism from violating the fully open toggle position, since the weight of the hanging perching mechanism is much less than the weight of the helicopter. We designed a hard mechanical stop to prohibit the mechanism from violating the fully open toggle position when hanging below the helicopter. The fully collapsed toggle position is avoided naturally through design, provided we do not attempt to perch on perches outside of (i.e., smaller than) the range for which the mechanism was designed.

The complete system prototype was created using two perching mechanisms (one mechanism per "foot") with each possessing three linkages and three toes, and these two mechanisms are joined to a common platform. To rigidly connect the platform to the helicopter, snap clips were created on the top of the platform to enable the platform to snap on to the helicopter's skids. We used the method of Sec. 4.2 to choose a base length of $b = 42$ mm, a toe length of $T = 28$ mm (which has a 5% factor of safety), and a rigid toe angle of $\Psi = 2.48$ rad (142 deg). For the link length of our mechanism, we arbitrarily chose the value $L = 25$ mm, and we verified that this value was less than the maximum value such that the total prototype weight, 20 g (including the two feet and the connecting/mounting platform) was still within the helicopter's payload (the maximum allowable value based on payload is $L = 45$ mm). Multiple iterations of the linkage design were explored to reduce mass and improve strength [30]. The links feature cross bracing to improve rigidity of the mechanism and multiple hinges at each joint to improve durability.

SolidWorks renderings of the final mechanism (i.e., a single foot), perching on the large and small perches, are shown in Fig. 12. The prototype was created in Objet Vero White Plus plastic using a 3D printer. Each joint was reamed using a 1.5-mm high-speed steel chucking reamer to place a low-friction pin joint that ensures free movement throughout the mechanism's ascent and descent onto a perch. Joints were also sanded down to minimize friction created from imperfections in the 3D printing. Table 1 shows the parameters used in the final mechanism design and analysis.

In order to increase the friction between the mechanism and the perch, we coated the toes and bottom plate of the mechanism in Mold Max 40 (Smooth-On, Easton, PA), which is a condensation-cure silicone rubber compound. The compound was mixed to data-sheet specifications and coated on the toes and base plate with a brush and then allowed to fully cure before first use.

The static coefficient of friction μ between the toes of the mechanism and the perch was found using a simple slip test between the material used to coat the toes and the material used for the perches. The static coefficient of friction was estimated by slowly inclining the two materials and measuring the angle φ above horizontal at which a slip occurs. The static coefficient of friction is

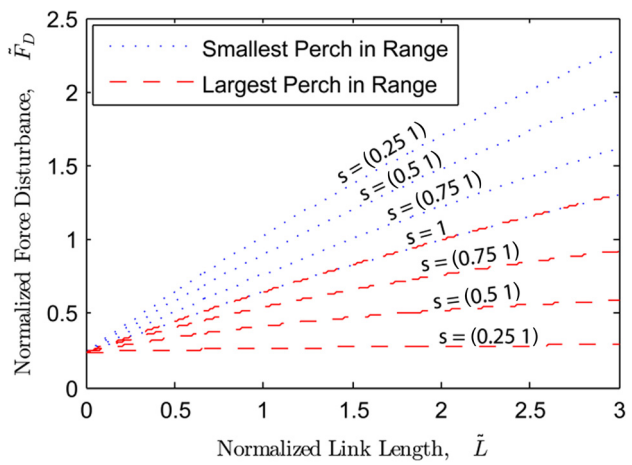

Fig. 10 Normalized force disturbance versus normalized link length for four different mechanisms that have each been optimized for a specified range of perch sizes (with $\theta_{\min} = \pi/18$ rad, and $\tilde{a} = 3.255$ in all cases). The range $s = 1$ corresponds to the optimal design for a single perch size.

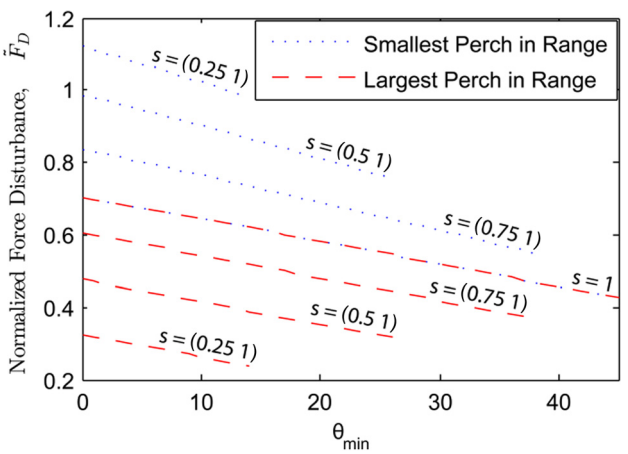

Fig. 11 Normalized force disturbance versus minimum grip angle (deg) for four different mechanisms that have each been optimized for a specified range of perch sizes (with $\tilde{L} = 1$, and $\tilde{a} = 3.255$ in all cases). The range $s = 1$ corresponds to the optimal design for a single perch size.

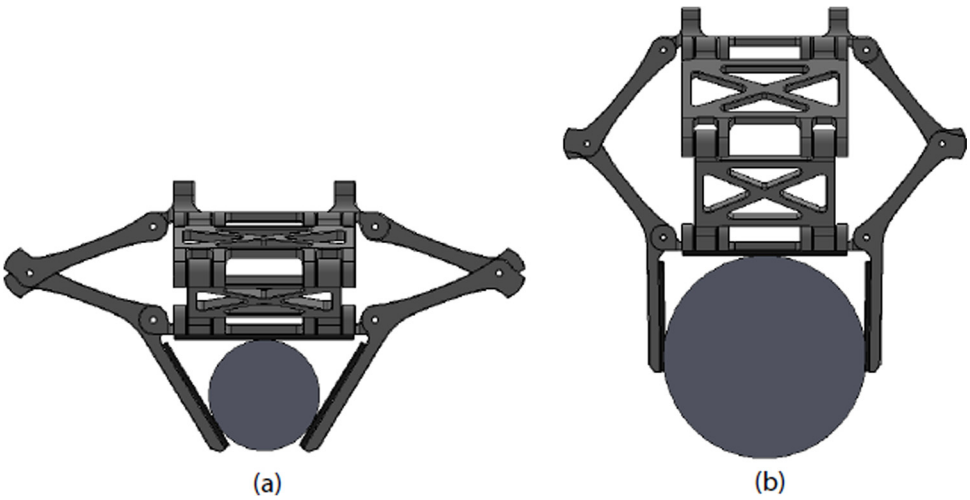

Fig. 12 Model of the prototype, optimized for the range of perch sizes of $s = [0.5\ 1]$: (*a*) the prototype on the smallest perch in range and (*b*) the prototype on the largest perch in range

Table 1 Parameters used for prototype design

Parameters	Values	Units
Weight of helicopter and mechanism system (W)	2.0	N
Coefficient of static friction (μ)	0.35	—
Link length (L)	0.025	M
Base (b)	0.042	M
Rigid toe angle (Ψ)	2.48	rad
Minimum grip angle ($\theta_{\min}$)	0.262	rad
Distance to center of pressure (a)	0.062	m

then calculated as $\mu = \tan(\varphi)$, which we measured by using the average of ten trials to have a value of $\mu = 0.35$.

To experimentally evaluate the disturbance-rejection capability of the perching mechanism, we conducted an experiment in which a string was attached to the back of the helicopter body at approximately the estimated location of the center of pressure. The string left the helicopter body horizontally and then was routed around a pulley, such that precision weights could be placed in a cup at the end of the string, and the downward force due to their weight is converted into a rearward horizontal force on the helicopter. For each of the large and small perches, an experiment was conducted in which the helicopter was manually perched and then weight was slowly added to the string until slip in the grip was observed. The force value was recorded, and the process was repeated for a total of ten trials per perch. For the largest perch, the disturbance

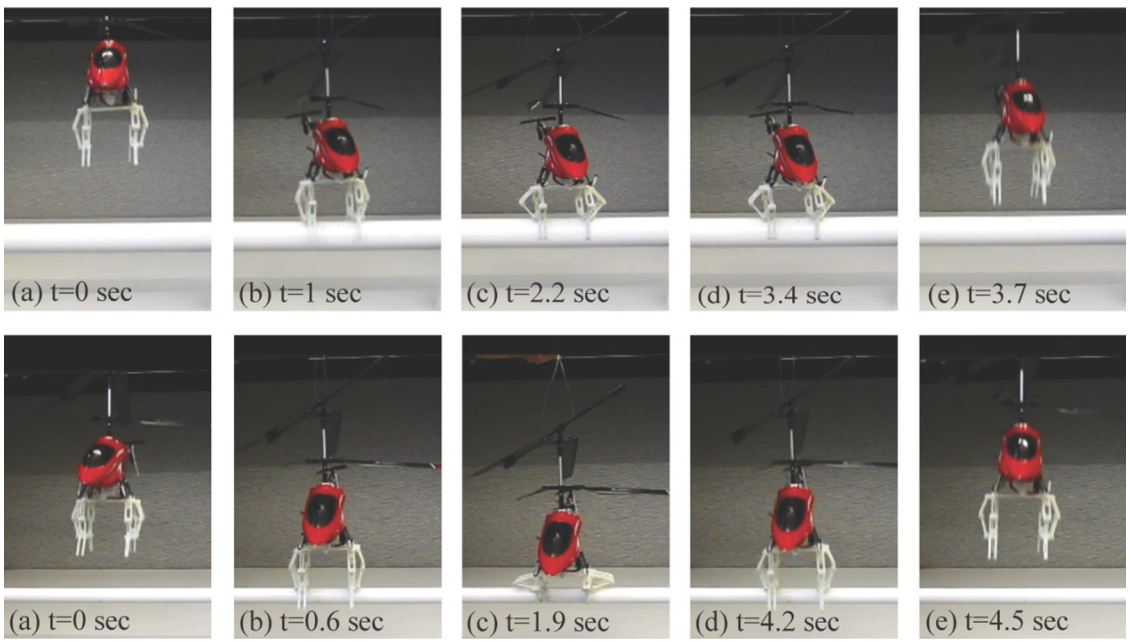

Fig. 13 Video images of the descent and ascent of helicopter with attached perching mechanism on 42 mm (top row) and 21 mm (bottom row) diameter PVC perches. The system is manually lowered onto the perch using a string in (*a*) and (*b*), the string is allowed to go completely slack in (*c*) to allow the complete weight of the helicopter to generate a grip and pause there, and then the string is used to lift the helicopter off the perch in (*d*) and (*e*). Top row: (*a*) $t = 0$ s, (*b*) $t = 1$ s, (*c*) $t = 2.2$ s, (*d*) $t = 3.4$ s, and (*e*) $t = 3.7$ s and bottom row: (*a*) $t = 0$ s, (*b*) $t = 0.6$ s, (*c*) $t = 1.9$ s, (*d*) $t = 4.2$ s, and (*e*) $t = 4.5$ s.

force (mean ± standard deviation) at which slip occurred was 324 ± 32 mN. This value of force corresponds to a wind speed of approximately 10.4 m/s (neglecting lift effects). For the parameters used in the prototype, based upon the combined weight of the helicopter and top plate being 2.0 N, our analytical model predicts a maximum disturbance of 300 mN, which underpredicts our actual experimental mean value by 7.4%, but was within the range of values experimentally obtained. For the smallest perch, the disturbance force at which slip occurred was 352± 34 mN. This value of force corresponds to a wind speed of approximately 10.8 m/s (neglecting lift effects). Our analytical model predicts a maximum disturbance of 400 mN, which overpredicts our actual experimental mean value by 13.6%. These experiments suggest that our analytical model is valid for the purposes of perching-mechanism design, although the model seems to slightly underpredict on the large perch and overpredict on the small perch. Note that an initial group of tests indicated that the mechanism could reject much larger disturbance forces on the small perch [29], but we examined the mechanism carefully and determined that some of the joints had been over-reamed. This produced backlash, allowing the mechanism to approach its toggle point where large grip forces occur. As a result, we remanufactured parts of the mechanism and arrived at the results reported above [30]. In Fig. 13, we show our mechanism enabling our helicopter to make successful perches on both the largest and smallest perch sizes in the desired range. In the demonstration, the helicopter is hung from a string like marionette and manually made to descend and ascend with minimal control.

In our analysis, we assumed that perching failure would be due to a wind disturbance coming from the front or back of the rotorcraft, causing the grip to slip and rotate. To confirm this assumption, we performed an additional experiment to test the ability to reject disturbances coming from the side, with the conjecture that much larger forces will be rejected from this direction. We repeated the hanging-weight experiment described above, but this time by attaching the string with the hanging weights to the side of the helicopter, but at approximately the same height relative to the perch. The results for ten trials were that the large perch rejects 571 ± 33 mN, and the small perch rejects 1068 ± 64 mN. These values represent a 75% increase for the large perch and 83% increase for the small perch compared to the back-weighted experiment described previously. These values confirm our assumptions that the helicopter is most vulnerable to wind disturbances from the front and back of the rotorcraft as opposed to from the side.

We also evaluated whether the mechanism could maintain a stable perch on various objects. These include but are not limited to (a) a toroid, (b) chair back, (c) skewed boards on the edge of a pallet, (d) rectangular railings, (e) flat carpet surface, (f) tree branches, (g) odd shaped rims of outdoor garbage cans, and (h) irregular edges of rocks. As Fig. 14 indicates, irregular width objects result in the feet closing different amounts and the vehicle tips slightly to one side. Standing on flat surfaces requires sufficient friction, hence carpet is successful, whereas slippery flat surfaces allow the toes to slip and close.

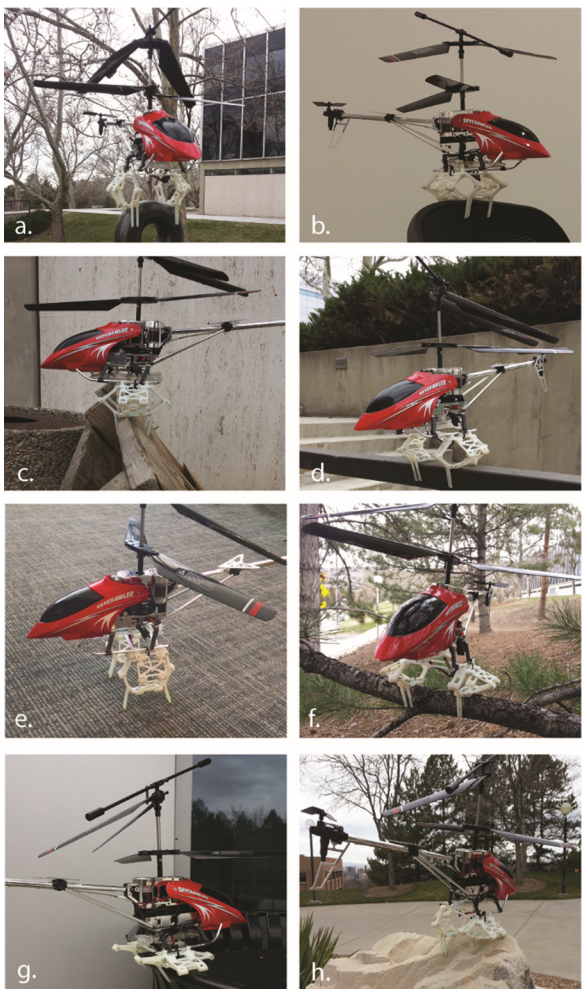

Fig. 14 Perching on various objects: (*a*) toroid, (*b*) chair back, (*c*) edge of pallet, (*d*) square railing, (*e*) human fingers, (*f*) tree branch, (*g*) edge of garbage can, and (*h*) edge of rock

6 Conclusion and Future Work

In this paper, we proposed a simple mechanism based on a Sarrus linkage that enables a rotorcraft to perch on cylindrical perches using only the weight of the rotorcraft to maintain a grip on the perch. We provided an analysis of the mechanism's kinematics, we presented the static force equations that describe how the weight of the rotorcraft is converted into grip force onto the perch, and we described how grip forces relate to the ability to reject horizontal disturbances such as wind gusts. The mechanism was optimized for use on a single perch size, and then for a range of perch sizes. We concluded by constructing a prototype mechanism optimized for a range of perches in which the smallest perch in the range is half the diameter of the largest perch in the range. We demonstrated the usefulness of the mechanism applied to a helicopter through a series of experiments, although any vehicle could have been used since the helicopter was not flying. For the helicopter, the mechanism was able to resist disturbances equivalent to wind speeds of 10 m/s by design, and the mechanism is light enough to be lifted by the helicopter without utilizing its entire payload capacity.

As the design process and results indicate, the largest perch size and resulting range of perch sizes is limited by the mass available for the mechanism and desired disturbance rejection. The mass of the top plate, bottom plate, and toes is proportional to the largest perch diameter. Increasing the range of perch sizes to allow for smaller perches results in reduced disturbance rejection on larger perches. Disturbance rejection can be improved by increasing link length, L. However, increasing perch size and disturbance rejection increases mechanism mass and the distance the mechanism protrudes below the rotorcraft. Ultimately, it is the designer's prerogative to design a mechanism that balances perch size, disturbance rejection, and mechanism size for their application.

In the future, it would be interesting to consider the same basic perching mechanism designed here, but without the assumption of straight rigid toes, which was made arbitrarily and for simplicity. It is possible that other toe geometries could lead to more desirable perching behavior. It would also be desirable to consider the use of different materials with higher strength-to-weight ratios, and to consider more optimized structural designs, again with the

goal of reducing weight. Finally, adding highly compliant high-friction padding to the toes and palm of the mechanism could enable better gripping of perches with little impact on the weight budget.

Acknowledgment

We would like to thank Tom Slowick for his assistance fabricating our prototypes and Kevin Marett for his assistance collecting wind-tunnel data. Partial student support was provided by the University of Utah Undergraduate Research Opportunity Program (UROP).

Nomenclature

a = height of disturbance force above top plate
$\tilde{a}$ = nondimensional height a with respect to r
b = base length
$\tilde{b}$ = nondimensional base length with respect to r
F_b = force between top plate and perch
F_D = disturbance force
$F_{D,max}$ = maximum disturbance force
F_t = force between toe and perch
$\tilde{F}_D$ = nondimensional $F_{D,max}$ with respect to μW
F_1 = force between top plate and Sarrus top link
$F_{1,1}, F_{1,2}$ = Cartesian components of F_1
h = mechanism height
L = link length
$\tilde{L}$ = nondimensional link length with respect to r
M_D = disturbance moment
$M_{D,max}$ = maximum disturbance moment
O_o = joint between lower Sarrus linkage and bottom plate
r = perch radius
s = dimensionless perch size relative to largest perch size
s_{min} = minimum dimensionless perch size
T = toe length
T_e = effective toe length
x_β = toe contact point x Cartesian location
y_β = toe contact point y Cartesian location
W = weight of aircraft
α = angle of symmetric halves of the area between a toe and the bottom plate
β = toe contact angle
θ = grip angle
μ = coefficient of friction
Ψ = rigid toe angle
$\Psi_{optimal}$ = optimal rigid toe angle

References

[1] Doyle, C. E., Bird, J. J., Isom, T. A., Johnson, C. J., Kallman, J. C., Simpson, J. A., King, R. J., Abbott, J. J., and Minor, M. A., 2011, "Avian-Inspired Passive Perching Mechanism for Robotic Rotorcraft," IEEE/RSJ International Conference on Intelligent Robots and Systems (IROS 2011), San Francisco, CA, Sept. 25–30, pp. 4975–4980.

[2] Doyle, C. E., Bird, J. J., Isom, T. A., Kallman, J. C., Bareiss, D. F., Dunlop, D. J., King, R. J., Abbott, J. J., and Minor, M. A., 2013, "An Avian-Inspired Passive Mechanism for Quadrotor Perching," IEEE/ASME Trans. Mechatronics, **18**(2), pp. 506–517.

[3] Wikipedia, 2013, "Sarrus Linkage," http://en.wikipedia.org/wiki/Sarrus_linkage

[4] Larson, A. J., 2011, "Development and Testing of an Active Perching System," Master's thesis, Oklahoma State University, Stillwater, OK.

[5] Moore, J., and Tedrake, R., 2011, "Magnetic Localization for Perching UAVs on Powerlines," IEEE/RSJ International Conference on Intelligent Robots and Systems (IROS 2011), San Francisco, CA, Sept. 25–30, pp. 2700–2707.

[6] Moore, J., and Tedrake, R., 2012, "Control Synthesis and Verification for a Perching UAV Using LQR-Trees," IEEE 51st Annual Conference on Decision and Control (CDC 2012), Maui, HI, Dec. 10–13, pp. 3707–3714.

[7] Hurst, A., Wickenheiser, A., and Garcia, E., 2008, "Localization and Perching Maneuver Tracking for a Morphing UAV," IEEE/ION Position, Location and Navigation Symposium (PLANS), Monterey, CA, May 5–8, pp. 1238–1245.

[8] Hurst, A., and Garcia, E., 2011, "Controller Design for a Morphing, Perching Aircraft," Proc. SPIE, **7977**, p. 79771L.

[9] Gomez, J. C., and Garcia, E., 2011, "Morphing Unmanned Aerial Vehicles," Smart Mater. Struct., **20**(10), p. 103001.

[10] Robertson, D. K., and Reich, G. W., 2014, "Design and Perching Experiments of Bird-Like Remote Controlled Planes," 54th AIAA/ASME/ASCE/AHS/ASC Structures, Structural Dynamics, and Materials Conference (SDM), Boston, Apr. 8–11, p. 17.

[11] Desbiens, A. L., Asbeck, A. T., and Cutkosky, M. R., 2011, "Landing, Perching and Taking Off From Vertical Surfaces," Int. J. Rob. Res., **30**(3), pp. 355–370.

[12] Desbiens, A. L., Asbeck, A. T., and Cutkosky, M. R., 2011, "Scansorial Landing and Perching," *Robotics Research*, Springer, Berlin, pp. 169–184.

[13] Glassman, E., Desbiens, A. L., Tobenkin, M., Cutkosky, M., and Tedrake, R., 2012, "Region of Attraction Estimation for a Perching Aircraft: A Lyapunov Method Exploiting Barrier Certificates," IEEE International Conference on Robotics and Automation (ICRA), St. Paul, MN, May 14–18, pp. 2235–2242.

[14] Anderson, M. L., Perry, C. J., Hua, B. M., Olsen, D. S., Parcus, J. R., Pederson, K. M., and Jensen, D. D., 2009, "The Sticky-Pad Plane and Other Innovative Concepts for Perching UAVs," 47th AIAA Aerospace Sciences Meeting, Orlando, FL, Jan. 5–8, AIAA Paper No. 2009-40.

[15] Cory, R., and Tedrake, R., 2008, "Experiments in Fixed-Wing UAV Perching," AIAA Guidance, Navigation, and Control Conference, Honolulu, HI, Aug. 18–21, AIAA Paper No. 2008-7256.

[16] Nagendran, A., Crowther, W., and Richardson, R., 2012, "Biologically Inspired Legs for UAV Perched Landing," IEEE Aerosp. Electron. Syst. Mag., **27**(2), pp. 4–13.

[17] Bachmann, R. J., Boria, F. J., Vaidyanathan, R., Ifju, P. G., and Quinn, R. D., 2009, "A Biologically Inspired Micro-Vehicle Capable of Aerial and Terrestrial Locomotion," Mech. Mach. Theory, **44**(3), pp. 513–526.

[18] Mellinger, D., Shomin, M., and Kumar, V., 2010, "Control of Quadrotors for Robust Perching and Landing," International Powered Lift Conference 2010, Philadelphia, PA, Oct. 5–7, pp. 119–126.

[19] Kovač, M., Germann, J., Hürzeler, C., Siegwart, R. Y., and Floreano, D., 2009, "A Perching Mechanism for Micro Aerial Vehicles," J. Micro-Nano Mechatronics, **5**(3–4), pp. 77–91.

[20] Mellinger, D., Shomin, M., Michael, N., and Kumar, V., 2012, *Cooperative Grasping and Transport Using Multiple Quadrotors* (Springer Tracts in Advanced Robotics), Springer, Berlin, pp. 545–558.

[21] Mellinger, D., Lindsey, Q., Shomin, M., and Kumar, V., 2011, "Design, Modeling, Estimation and Control for Aerial Grasping and Manipulation," IEEE/RSJ International Conference on Intelligent Robots and Systems (IROS), San Francisco, CA, Sept. 25–30, pp. 2668–2673.

[22] Pounds, P. E., Bersak, D. R., and Dollar, A. M., 2012, "Stability of Small-Scale UAV Helicopters and Quadrotors With Added Payload Mass Under PID Control," Auton. Robots, **33**(1–2), pp. 129–142.

[23] Ghadiok, V., Goldin, J., and Ren, W., 2012, "On the Design and Development of Attitude Stabilization, Vision-Based Navigation, and Aerial Gripping for a Low-Cost Quadrotor," Auton. Robots, **33**(1–2), pp. 41–68.

[24] Thomas, J., Polin, J., Sreenath, K., and Kumar, V., 2013, "Avian-Inspired Grasping for Quadrotor Micro UAVs," ASME Paper No. DETC2013-13289.

[25] Danko, T. W., Kellas, A., and Oh, P. Y., 2005, "Robotic Rotorcraft and Perch-and-Stare: Sensing Landing Zones and Handling Obscurants," 12th International Conference on Advanced Robotics (ICAR '05), Seattle, WA, July 18–20, pp. 296–302.

[26] Goldin, J. C., 2011, "Perching Using a Quadrotor With Onboard Sensing," Master's thesis, Utah State University, Logan, UT.

[27] Daler, L., Klaptocz, A., Briod, A., Sitti, M., and Floreano, D., 2013, "A Perching Mechanism for Flying Robots Using a Fibre-Based Adhesive," IEEE International Conference on Robotics and Automation (ICRA), Karlsruhe, Germany, May 6–10, pp. 4433–4438.

[28] Culler, E. S., Thomas, G. C., and Lee, C. L., 2012, "A Perching Landing Gear for a Quadcopter," AIAA/ASME/ASCE/AHS/ASC Structures, Structural Dynamics and Materials Conferecne, Honolulu, HI, Apr. 23–26, AIAA Paper No. 2012-1722.

[29] Burroughs, M. L., 2014, "A Sarrus-Based Passive Mechanism for Rotorcraft Perching," Master's thesis, University of Utah, Salt Lake City, UT.

[30] Freckleton, K. B., 2015, "Sarrus-Based Passive Mechanism for Rotorcraft Perching: Structural Design and Mass Optimization," B.S. Senior Honors thesis, University of Utah, Salt Lake City, UT.